Journal of Nanophotonics

SPIEDigitalLibrary.org/jnp

Terahertz-to-infrared converter based on metal nanoparticles: potentialities of applications

Kamil A. Moldosanov
Valery M. Lelevkin
Peter V. Kozlov
Andrey K. Kaveev

SPIE

Terahertz-to-infrared converter based on metal nanoparticles: potentialities of applications

Kamil A. Moldosanov,[a] Valery M. Lelevkin,[a] Peter V. Kozlov,[a] and Andrey K. Kaveev[b]

[a]Kyrgyz-Russian Slavic University, 44 Kiyevskaya Street, Bishkek 720000, Kyrgyzstan
altair1964@yandex.ru

[b]TYDEX® J.S.Co., 16 Domostroitelnaya Street, Saint Petersburg 194292, Russia

Abstract. In a new type of terahertz (THz)-to-infrared converter for the visualization of THz radiation sources, nanoparticles are embedded in a THz-transparent matrix material. The nanoparticles are made of a metal or an alloy having a partially filled peak of the electron density of states at the Fermi energy. The converter is designed to operate with the THz objective forming a source's image on the matrix, wherein the irradiated nanoparticles convert THz energy to thermal energy, whose spatial distribution is captured by an infrared camera. Nickel nanoparticles are very appropriate for high-frequency THz radiation and can find application in real-time passive imaging of biomedical objects at room temperature. Nanoparticles of compounds with heavy fermions are suitable for low-frequency THz radiation, which could be used to image concealed objects carried by a human being. [DOI: 10.1117/1.JNP.6.061716]

Keywords: terahertz to infrared converter; terahertz imaging; passive imager; imaging radar; nanoparticle.

Paper 12060SS received Jun. 5, 2012; revised manuscript received Nov. 27, 2012; accepted for publication Nov. 28, 2012; published online Dec. 13, 2012.

1 Introduction

Progress in terahertz (THz) optics and commercial availability of infrared imaging cameras with ~14 mK thermal sensitivities allow us to propose a simple way for imaging the objects-sources of THz radiation. In this way, the THz objective forms an image of the object on a two-dimensional THz radiation-to-heat converter. The converter represents a matrix of material transparent in THz rays with embedded nanoparticles of metal or alloy with a partially filled peak of the electronic density of states (DOS) at the Fermi energy. Nanoparticles being heated by THz radiation convert the THz energy to heat, and the two-dimensional pattern formed by heated nanoparticles in the converter is visualized by an infrared camera. The goal of this study was to determine the feasibility of the scheme for passive imaging through clothes to detect concealed objects, as shown in Fig. 1. The emergence of highly sensitive infrared (IR) cameras (~14 to 50 mK),[1] as well as the manufacturing of THz optical elements on a commercial scale,[2] would allow for testing of such a scheme.

In this scheme, the THz objective forms in THz rays the image of the object-source on the two-dimensional converter, converting the THz radiation to heat, i.e., to IR radiation. The image formed by the converter (now in IR rays) in turn serves as the object for the objective of the IR camera. The filter examines the object's heat radiation (for the body temperature $T \approx 300$ K, see Fig. 2; the filtered wavelengths should be $\lambda \sim 3$ to 30 μm, with the radiation peak at $\lambda \approx 10$ μm).

In contrast to the approach used by Luukanen et al. for passive THz imaging,[3–5] our approach is simpler and does not require the cryostat, vacuum subsystem, complex optics, readout electronics, data processing and data interfaces, and power supplies. Kuznetsov et al. used the THz-to-IR converter with a topological pattern of split-ring resonators.[6–8] Its disadvantages are the "comet tail" and image blooming effects, which deteriorate the converter's response time and

0091-3286/2012/$25.00

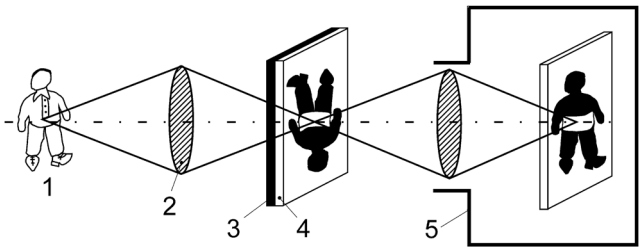

Fig. 1 Scheme for visualizing the THz radiation source. 1: object-source of the THz radiation, 2: THz objective of polyethylene HDPE (See Ref. 2), 3: heat filter (See Ref. 2), 4: THz-to-IR converter matrix, 5: IR camera *Mirage P* (See Ref. 1).

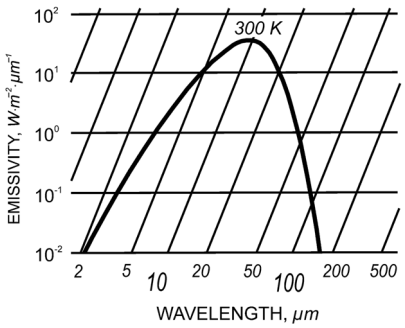

Fig. 2 Black body radiation at temperature 300 K. We briefly approximated the human body's radiation by this distribution halved.

spatial resolution. Due to the use of nanoparticles, our THz-to-IR converter is expected to be free of these disadvantages. Moreover, estimations promise other advantages over the Kuznetsov's group converter. The operating THz power is about an order of magnitude less than that in their works, and the THz-to-IR converter's area is ≈3.5 times larger than their converter's area.

2 THz-to-IR Converter: Estimates of Technical Parameters

In metal particles, as their dimensions decrease, the energy levels of electrons become separated up to values typical for energies of THz quanta. This size effect can be used to absorb the THz radiation. Besides, in nanoparticles, because of the uncertainty relation, the uncertainty in the momentum of the Fermi electrons exceeds the value of the momentum Δp, which should be transferred from the photon to the electron for their interaction to happen. (The photon's momentum p_{ph} is not enough for the photon-electron interaction, because $p_{\mathrm{ph}} < \Delta p$.) Thus, the uncertainty in the momentum of the Fermi electrons ensures the fulfillment of the momentum conservation law and ultimately the absorption of the photon's energy.

If one introduces a proper number of metal particles into the matrix transparent in THz rays, the THz radiation could heat the particles up to the sensitivity thresholds of contemporary IR cameras.

The transition metal with the DOS peak at E_F is preferable as the material for nanoparticles-converters. As it is in all metals, due to heat excitations, part of electron states below the Fermi energy, within the energy band from $E_F - 0.5 \cdot \mathrm{kT}$ (where k is the Boltzmann constant, $T \approx 300$ K, and $\mathrm{kT} \approx 26$ meV) to E_F, becomes unoccupied. The electrons transit from these states to the ones above the Fermi energy within the band from E_F to $E_F + 0.5 \cdot \mathrm{kT}$. As a result, the electrons within the band of width kT near the E_F become able to absorb the photon energies, i.e., to be excited to the energy states above the initial ones up to the upper edge of the d-band. Being scattered, these electrons are returned to unoccupied states within the band of width kT.

Choosing for particles the transition metal with the DOS peak at E_F promises a gain in the number of electrons able to absorb photons. Besides, this choice promises an enhanced scattering intensity of excited electrons. Therefore, the energy transfer from photons to ions of metal will be

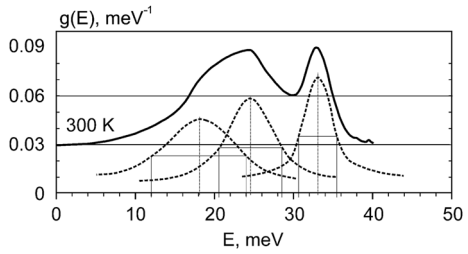

Fig. 3 Phonon DOS in Ni at temperature $T = 300$ K (solid line, reproduced from Refs. 9 and 10). The dashed lines show approximate resolution of the phonon DOS curve into three components.

more intensive, and nanoparticles could be heated to a higher temperature than nanoparticles of ordinary metal.

Our approach is based on usage of Ni nanoparticles. Distribution of phonon DOS in Ni at $T = 300$ K (Fig. 3) matches well with the emissivity distribution of the black body radiation at $T = 300$ K (Fig. 2), namely, the phonon DOS is maximum or enhanced just within the energy band ~10 to 35 meV, where the contribution of THz photons into the black body emissivity is maximum or large (wavelengths ~30 to 150 μm or, in energy units, ~10 to 40 meV).

In Ni, a width of the 3d-band is about 5.5 eV, with part of the 3d-band above the Fermi energy (Fig. 4), which determines an intensive electron scattering in this metal. Compared to other metals, Ni has maximum electronic DOS at the Fermi energy.[11]

In Sec. 2.1, the average dimension of Ni particles is adopted to be about 2.4 nm. As it is less than the free path length of electron (≈4 nm), a presence of the DOS peak at the Fermi energy of Ni increases a probability of electron scattering on the nanoparticle's surface and ultimately the probability of transfer of energy gained by electron from photon to ions of the nanoparticle.

In Ni, the upper edge of the 3d-band is above the Fermi energy by roughly 0.5 eV. Thus, the Ni nanoparticles are able to convert to heat the photon energies of entire THz range. However, this wide band absorptivity is attended with an unacceptable feature: since the upper edge of the 3d-band is above E_F by 0.5 eV, the converter's nanoparticles can be heated by IR photons with energies up to 0.513 eV (wavelengths ≥2.42 μm). Therewith, the photons most dangerous from the viewpoint of background noise, corresponding to $\lambda \approx 10$ μm, can get within the absorption band. That is why a filter is needed to protect the converter's nanoparticles from unacceptable heating; it should filter a spurious IR radiation with $\lambda < 30$ μm from the object-source but pass its useful (wanted) THz radiation with $\lambda \geq 30$ μm.

2.1 *Estimation of Size of Ni Nanoparticles*

The choice of size for the Ni particles was based on analysis of the phonon DOS distribution in energy at temperature $T = 300$ K.[9,10,13] We used the distribution from Kresch and Kresch et al.[9,10] and resolved it approximately into three peaks (dashed lines in Fig. 3).

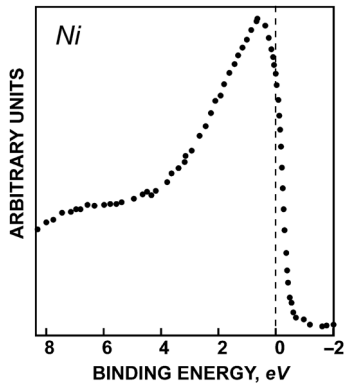

Fig. 4 Electronic density of states in Ni (See Ref. 12). The vertical dash line indicates the Fermi energy position.

Table 1 Parameters of three subdistributions of the phonon DOS in Ni at $T = 300$ K.

Energies of peaks of subdistributions (meV)	Energies corresponding to FWHM edges (meV)	Wavelengths corresponding to FWHM edges (μm)	Diameter D of nanoparticles (nm)
$E_1 = 18$	12	103.4	3.0
	24	51.7	
$E_2 = 24.5$	20.5	60.5	2.4
	28.5	43.5	
$E_3 = 33$	30.5	40.7	2.2
	35.5	34.9	

According to peaks of subdistributions, three diameters D of nanoparticles were estimated (Table 1). We assumed that particles with these diameters were "tuned" to the most probable frequencies of ion vibrations in nanoparticles. Approximately, one may think that nanoparticles of such diameters absorb most of the THz range. Correspondingly, in estimations, one should take the minimum energies of the FWHM edges, namely 12, 20.5, and 30.5 meV, as the minimum energies between electron energy states. Then nanoparticles of these subdistributions will absorb photons with energies multiple of, correspondingly, 12, 20.5, and 30.5 meV. The THz energies will be absorbed discretely. However, in reality, because of the spread in sizes of real nanoparticles, the absorbed spectrum will be quasi-continuous. In our estimations, we took into account the discreteness of the absorbed THz spectrum through the blackness α. Besides, we did the next step in approximations. When estimating the surface densities of Ni nanoparticles in the converter, we assumed roughly that all nanoparticles had the same minimum FWHM edge phonon energy of 20.5 meV.

Let us estimate now how many atoms N of nickel should be contained in the particle so that the energy gap between the electron levels in the 3d-band are equal to the average minimum FWHM edge phonon energy of 20.5 meV. The total number of electron energy levels in the 3d-band is equal to number of atoms in the particle. Then the following equation is valid: $N - 1 = 5.5\ \text{eV}/2.05 \cdot 10^{-2}\ \text{eV} = 268$.

Thus, $N = 269$. As a lattice in Ni is the face-centered cubic one with four atoms per unit cell, a number of cells in the particle consisting of 269 atoms equals $n \approx 269/4 \approx 67$. Assume that the Ni particle is a cuboid. Then the number of cells in the particle's edge is equal to $l = (67)^{1/3} \approx 4$. The lattice constant of Ni is 3.52 Å,[14] so the value of the particle's edge equals $l \approx 4 \cdot 3.52$Å ≈ 1.4 nm, and its body diagonal (particle "diameter" D) equals $(3)^{1/2} \cdot l \approx 1.73 \cdot 1.4\ \text{nm} \approx 2.4$ nm.

2.2 *Estimations of Powers Required to Hold Nickel Nanoparticles at Temperatures Defined by Their Blackness α*

The problem was solved of temperature change in a Ni particle placed inside a gelatin spherical shell as a result of heat releasing in the particle. The temperature change in the Ni particle was described by the heat conduction equation in spherical coordinates with the source function $q(r)$ taken into account:

$$\rho C \frac{\partial T}{\partial t} = \frac{1}{r^2} \frac{\partial}{\partial r} \left(\lambda r^2 \frac{\partial T}{\partial r} \right) + q(r), \tag{1}$$

where T is the temperature, ρ is the volume density, C is the specific heat, λ is the heat conductivity, q is the volume density of the heat source, and r is the spherical radius.

It was thought that the thermal parameters did not depend on temperature and might be prescribed as

$$\begin{aligned} &0 \le r \le R_0: \quad \lambda = \lambda_1, \quad \rho = \rho_1, \quad C = C_1, \quad q = \tfrac{Q}{(4/3)\pi R_0^3}, \\ &R_0 < r \le R: \quad \lambda = \lambda_2, \quad \rho = \rho_2, \quad C = C_2, \quad q = 0, \end{aligned} \tag{2}$$

where R_0 is the radius of the nanoparticle, and R is the radius of the gelatin shell ($R \gg R_0$; in this problem, $R = 5 \cdot 10^{-7}$ m; this choice was justified by the fact that gelatin prevailed in the converter's volume).

The initial and edge conditions were

$$T(0, r) = T_R, \quad \left.\frac{\partial T(t, r)}{\partial r}\right|_{r=0} = 0, \qquad T(t, R) = T_R. \tag{3}$$

A solution for Eqs. (1)–(3) was sought by the numerical method of lines[15,16] relative to $\Delta T = T - T_R$, where $T_R = 300$ K. To control the accuracy and time of calculations, we used the steady-state resolution of the problem:

$$\frac{1}{r^2}\frac{d}{dr}\left(\lambda r^2 \frac{dT}{dr}\right) + q(r) = 0, \qquad T'(0) = 0, \qquad T(R) = T_R,$$

which gave a relationship between power Q and a maximum temperature rise ΔT_m:

$$\Delta T_m = \frac{Q}{8\pi}\left(\frac{1}{R_0\lambda_1} + \frac{2}{R_0\lambda_2} - \frac{2}{R\lambda_2}\right).$$

On reaching the value of $\Delta T = 0.995 \cdot \Delta T_m$, the heat source was turned off, and the problem was solved by cooling the Ni particle down to 300 K. Numerical calculations were carried out with the material parameters given in Table 2.

We calculated the values of power Q required for heating a Ni nanoparticle with a size of 2.4 nm for different temperature rises ΔT_m (see Fig. 5) in steady state. Values of Q_i for five values of blackness α_i are given in Table 3.

Table 2 Parameters of materials used in estimations.

Material	Volume density (g/cm^3)	Specific heat (J/kg · K)	Heat conductivity (W/m · K)
Nickel	$\rho_1 = 8.9$	$C_1 = 440$	$\lambda_1 = 90.9$
Gelatin	$\rho_2 = 1.3$	$C_2 = 1900$	$\lambda_2 = 0.3$

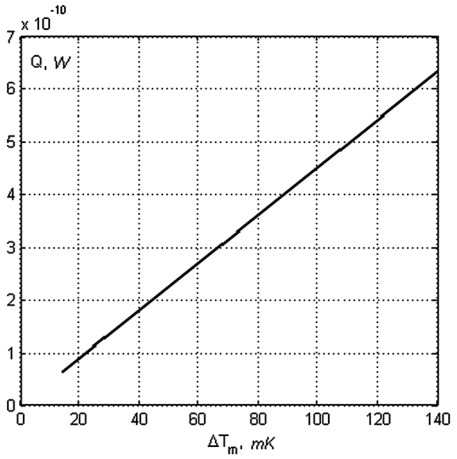

Fig. 5 Power Q against the temperature rise ΔT_m for Ni nanoparticle of radius $R_0 = 1.2$ nm in gelatin spherical shell.

Table 3 THz-to-IR converter's parameters at different blackness α_i of Ni nanoparticles.

	α_i				
Converter's parameters	1	0.7	0.5	0.3	0.1
ΔT_m, mK	14	20	28	46.7	140
Q_i, W	$6.34 \cdot 10^{-11}$	$9.05 \cdot 10^{-11}$	$1.27 \cdot 10^{-10}$	$2.11 \cdot 10^{-10}$	$6.34 \cdot 10^{-10}$
N_i, mm^{-2}	$2.71 \cdot 10^3$	$1.90 \cdot 10^3$	$1.35 \cdot 10^3$	$8.13 \cdot 10^2$	$2.71 \cdot 10^2$
H, m	3.43	3.11	2.82	2.42	1.68

2.3 *Estimations of Converter's Time Characteristics*

Contrary to Kuznetsov's group converter, which operates in a real-time scale and has the dimensions of heat-generating elements $\approx 100 \times 100$ μm^2, in our converter, the heat-generating elements, i.e., Ni nanoparticles, are much smaller. Therefore, we expected to obtain the time characteristics of our converter enabling operation in a real-time scale, too.

By the numerical method of lines,[15] with the program,[16] the time characteristics of the THz-to-IR converter were determined. For a Ni nanoparticle with a size of 2.4 nm in gelatin spherical shell, for five values of power Q_i from Table 3, we estimated the heating and cooling times (for initial temperature 300 K). The results are shown in Fig. 6. These times were found to be about 13 ns, which certainly enable operating the considered THz-to-IR converter in a real-time scale in both passive and active mode.

2.4 *Estimations of Radial Distributions of Temperature*

With the program,[16] we also determined the radial distributions of temperature for a Ni nanoparticle of radius $R_0 = 1.2$ nm in gelatin spherical shell for five values of Q_i from Table 3 (see Fig. 7). The distributions demonstrated that application of Ni nanoparticles might ensure that the "comet tail" and image blooming effects inherent in the approach by Kuznetsov et al. could be avoided. Hence, the converter's response time and spatial resolution could not be affected.

Figure 7 shows that, when $\alpha_i = 0.5$ (heating by $\Delta T = 28$ mK), the temperature of heating gelatin with reference to 300 K decreases almost to zero within a radius of about 40 nm. That is, beyond the radius of 40 nm, gelatin is not heated. At the concentrations of Ni nanoparticles in gelatin we are considering, the nanoparticles' size ($\approx$2.4 nm) is almost four orders of magnitude less than the distances between them. Therefore, the overlapping of temperature fields of heated nanoparticles is negligible. As a result, the "comet tail" and image blooming effects are impossible.

In the Kuznetsov's group converter, the dimensions of heat-generating elements $\approx 100 \times 100$ μm^2 with gaps between them of about 10 μm, i.e., a length of heated element is an

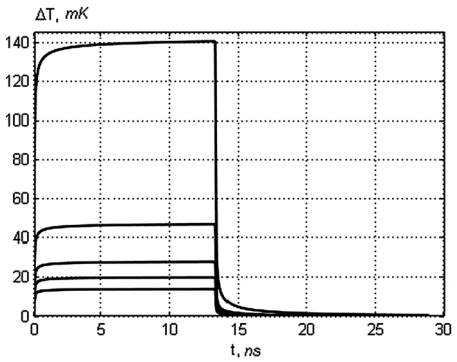

Fig. 6 Temperature rise ΔT versus heating/cooling time t for a Ni nanoparticle of radius $R_0 = 1.2$ nm in gelatin spherical shell for five values of Q_i from Table 3.

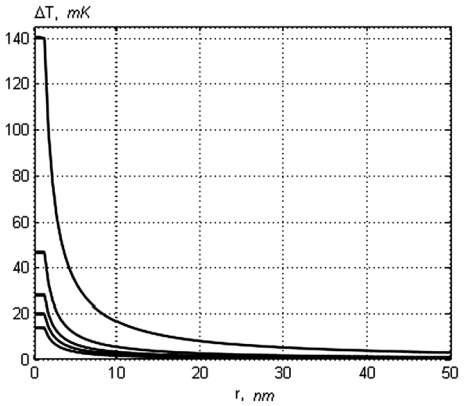

Fig. 7 Radial distributions of temperature for a Ni nanoparticle of radius $R_0 = 1.2$ nm in gelatin spherical shell for five values of Q_i from Table 3.

order of magnitude greater than the gap. Obviously, the temperature fields of heated elements overlap, resulting in the image blooming effect. A similar effect was described by Keblinski et al.[17]

2.5 *Estimation of Surface Density of Ni Nanoparticles*

Starting from the temperature sensitivity of the IR camera, let us estimate a surface density of Ni nanoparticles in the converter required to realize a passive imaging of the human body.

Evidently, the temperature sensitivity ΔT_{bb} given in specifications of IR cameras is related to radiation of the absolutely black body. Then the camera's susceptibility threshold in the surface power density equals $\Delta\varepsilon_\lambda = 4\sigma \cdot T^3 \cdot \Delta T_{\text{bb}}$, where σ is the Stefan-Boltzmann constant, and $T = 300$ K. At $\Delta T_{\text{bb}} = 14$ mK, $\Delta\varepsilon_\lambda = 8.58 \cdot 10^{-8}$ W/mm^2. This means that, for the surface of blackness α to be visible to the IR camera, a rise in its surface power density should be equal to or greater than $\Delta\varepsilon_\lambda = 8.58 \cdot 10^{-8}$ W/mm^2, while the temperature rise should be equal to or greater than $\Delta T = \Delta T_{\text{bb}}/\alpha$.

In Fig. 5, the values of power Q are given that are required to hold the 2.4-nm Ni nanoparticle in gelatin matrix at temperatures of 300 K + ΔT_m. In steady state, the nanoparticle releases a power of $Q/2$ into a half-space with the IR camera. Therefore, the surface density of a number of Ni nanoparticles on the converter's surface equals $N_i = \Delta\varepsilon_\lambda/(Q_i/2)$. These values for different α_i are given in Table 3.

2.6 *Estimation of the THz Power Delivered from the Human Body to the Converter*

The THz power P delivered from the human body to the converter can be estimated as

$$P \approx S_s \cdot \Omega \cdot T_{\text{tot}} \cdot T_{\text{air}} \cdot 0.5 \cdot c^2 \cdot h \cdot \int_{34.9}^{103.4} \frac{d\lambda}{\lambda^5 \cdot [\exp(47.97/\lambda) - 1]},$$

where S_s is an effective area of the human body's surface that emits THz radiation toward the THz objective, $S_s \approx 1.1 \cdot 10^{12}$ μm^2. (We have estimated it as the area of the half-cylinder of diameter 40 cm and height 175 cm.); Ω is a solid angle wherein the human sees the THz objective's diameter. (For definiteness, we have chosen the THz objective's diameter equal to 30 cm.); T_{tot} is a total transmittance of the THz objective and heat filter.[2] (We have estimated its value as $T_{\text{tot}} \approx 0.08$ nearby the wavelength range $\sim$30 μm, which contributes the most emissivity to the total human body's THz radiation.); T_{air} is a transmittance of the air layer between the human and the THz objective; 0.5 is a factor introduced to take roughly into account the fact that the human body is not the absolutely black body; $\int_{34.9}^{103.4} \frac{d\lambda}{\lambda^5 \cdot [\exp(47.97/\lambda)-1]} = 8.91 \cdot 10^{-8}$ μm^{-4} is

Table 4 Comparative data of two approaches to THz imaging using the THz-to-IR converters.

Parameters of the THz imaging system	Kuznetsov et al. (Refs. 6–8) (experiment)	Our approach (estimations)
Operating mode	Active	Passive and/or active
THz radiation source	Backward wave oscillator BWO-30	Human body or radiation source
Power required for operating, mW	5	0.5
Type of heat-generating element	Split-ring resonator	Ni nanoparticle
Sizes of heat-generating element	$\approx 100 \times 100\ \mu m^2$	Diameter ≈ 2.4 nm
IR camera's NETD, mK	100	14
THz-to-IR converter's area, mm^2	804.25	2,940

an integral between the limits 34.9 and 103.4 μm of the function describing distribution of the black body radiation in wavelengths. (Here, a number 47.97 is the value of hc/kT, expressed in μm, where h and k are correspondingly the Planck and Boltzmann constants, c is the light velocity, and T is temperature.) The integration limits are defined in Sec. 2.1 (see Table 1).

Thus, the human body's THz power delivered to the gelatin matrix with embedded Ni nanoparticles is equal to $P \approx 0.23\ \Omega \cdot T_{\text{air}}$, W. At average values of $\alpha_i = 0.5$ and $H = 2.82$ m, the solid angle $\Omega = 8.9 \cdot 10^{-3}$ sr and the transmittance $T_{\text{air}} \approx 0.245$, hence, $P \approx 0.5$ mW. For comparison, in Table 4, the data are given on the THz imaging system experimentally tested by Kuznetsov et al.,[6–8] along with the estimated data of our approach. Kuznetsov's group used a monochromatic (0.3 THz) radiation source with an emission power of 5 mW and an IR camera with the noise equivalent temperature difference (NETD) of 100 mK. Thus, our estimations show that, by using Ni nanoparticles as heat-generating elements in the THz-to-IR converter and a contemporary IR camera with a NETD of 14 mK, it is possible to heat the converter's nanoparticles with the human body's THz power of 0.5 mW only, which is an order of magnitude less than the source's power in the experiments of Kuznetsov's group. Besides, it should be noted that our THz-to-IR converter's area is $\approx$3.5 times larger.

2.7 *Estimation of the Converter's Effective Area*

Starting from the THz power distribution of the human body, let us estimate an effective area of the converter S^*, able to be heated by temperature $\Delta T = \Delta T_{\text{bb}}/\alpha$. The effective area equals $S* = \alpha \cdot P/\Delta\varepsilon_\lambda = \alpha \cdot P/4\sigma \cdot T^3 \cdot \Delta T_{\text{bb}}$. Here, P is the THz power delivered from the human body to the converter. Then the effective area that can be heated by human body's THz power equals

$$S* = \alpha \cdot P/\Delta\epsilon_\lambda = 5.75 \cdot 10^{-2} \cdot \alpha \cdot \Omega \cdot T_{\text{air}}/\sigma \cdot T^3 \cdot \Delta T_{\text{bb}}.$$

2.8 *Estimation of the Converter's Geometric Area*

Starting from data of the standard objective of the *Mirage P* IR camera, let us determine geometrical dimensions of the converter and its area visible to the camera. According to web site data,[1] a minimum distance d between the object (in our case, the THz-to-IR converter) and the camera's objective equals 4 in. i.e., $d = 101.6$ mm. With the field of view angle $\gamma = 26$ deg, a height h of the converter equals $2d \cdot \text{tg}(\gamma/2) \approx 47$ mm. With a standard aspect ratio of 4:3, a width w of the converter equals $(4/3) \cdot 47\ \text{mm} = 62.65$ mm. Thus, the converter's area is equal to

$$S_{\text{conv}} = 47\ \text{mm} \times 62.65\ \text{mm} = 2.94 \cdot 10^3\ \text{mm}^2.$$

2.9 *Estimation of the Operating Distance*

Let us determine the operating distance H between the THz objective and the object-source of the THz radiation by equating the converter's area S_{conv} and the effective area S* that can be heated by the human body's THz power by temperature $\Delta T = \Delta T_{\text{bb}}/\alpha$. Then

$$5.75 \cdot 10^{-2} \cdot \alpha \cdot \Omega \cdot T_{\text{air}}/\sigma \cdot T^3 \cdot \Delta T_{\text{bb}} = 2.94 \cdot 10^3 \text{ mm}^2. \quad (4)$$

In this equation, both the solid angle Ω and the air transmittance T_{air} are functions of the distance H. We chose the THz objective lens's radius of 0.15 m, whereas the air transmittance T_{air} was determined experimentally (Fig. 8). By calculating the value of Ω and estimating the value of T_{air} for the same value of H, and then substituting them in Eq. (1), one can determine the value of H that meets Eq. (4). Assume in accordance with Fig. 8 that, within the wavelength range from 30 to 250 μm, the average air transmittance of the 1.2-m air path is roughly equal to 0.55. Then for any distance H, the air transmittance equals $T_{\text{air}} \approx (0.55)^k$, where $k = H/(1.2 \text{ m})$.

Let us choose for conclusion an average value of $\alpha_i = 0.5$. A distance $H = 2.82$ m in Table 3 shows that, due to absorption in air, the approach with Ni nanoparticles cannot provide passive THz imaging for security applications. The distance is too small, whereas the security applications usually require distances of 4 to 20 m. In addition, Fig. 9 shows that clothes absorb entirely the human body's high-frequency THz radiation. Meanwhile, the Ni nanoparticles convert well just the high-frequency part of the THz range.

However, the approach with Ni nanoparticles is suitable for the passive THz imaging in medicine at short distances between the patient and the THz objective.

The considered approach can be used for active real-time standoff detection of weapons and contraband, if the THz-to-IR converter operates in a submillimeter- or millimeter-wave range, where transmittance of clothes is sufficiently high. In this case, it is preferable to use the nanoparticles of alloys with heavy fermions, rather than Ni nanoparticles, in the converter. The nanoparticles of heavy-fermion alloys are able to convert efficiently just the long-wave THz radiation into heat.[18] These compounds are considered in more detail in the appendix.

Kemp[19] explored the progress over the past 10 years toward the practical development of THz spectroscopy as a technique for concealed explosives detection and concluded that imaging at low-frequency THz radiation would be a more promising technique for security applications. This accords with our conclusion that the considered THz-to-IR converter would be applicable in submillimeter- and millimeter-wave imaging radars.

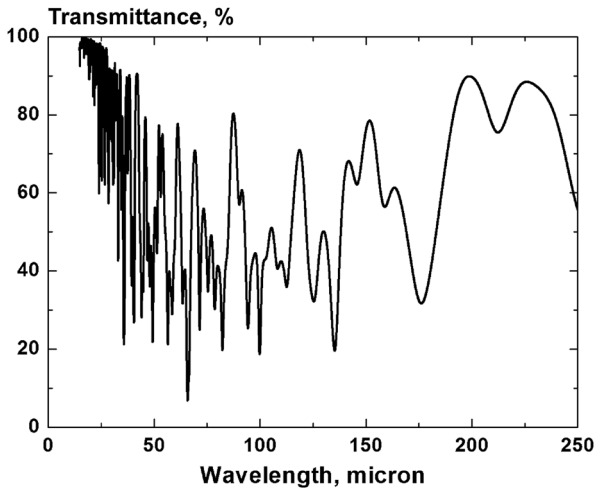

Fig. 8 Transmittance of the 1.2-m air path under normal conditions.

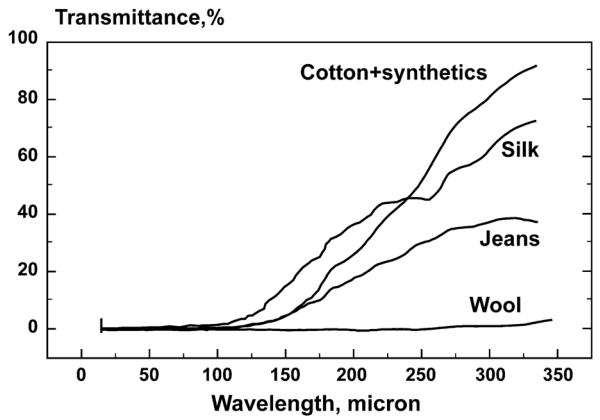

Fig. 9 Transmittance of different clothes versus wavelength.

3 Conclusion

For visualizing the objects concealed under clothing, the advantages of THz radiation, typical for adjacent ranges of the electromagnetic spectrum, can be used. Like radio-frequency waves, low-frequency THz radiation can transmit through materials opaque for visible rays (i.e., clothing), and like IR waves, THz rays can be refracted and focused by lenses. For imaging outlines of hidden metal articles, we can use another property of THz radiation: its ability to be reflected by metals.

The visualization scheme is proposed with a THz-to-IR converter containing nanoparticles of a metal or compound with the peak of the density of electron states at the Fermi energy. The Ni nanoparticles could be used as converters of high-frequency THz radiation in passive imaging of medical objects. The nanoparticles of compounds with heavy fermions could be used as converters of low-frequency THz radiation in active security applications. In this THz-to-IR converter, the time characteristics make possible real-time imaging in both passive and active modes. Combination of these characteristics with the converter's ability to work at room temperature opens new potentialities of applications in both crime fighting and early cancer diagnostics.

Appendix: Nanoparticles of Compounds With Heavy Fermions as the THz-to-IR Converters

In bulk compounds with heavy fermions (CHF),[20] like $CePd_3$, $CeAl_3$, $CeCu_6$, etc., at low temperatures ($10 - 100$ K), due to a narrow and partly occupied f-band of electrons at the Fermi energies, the DOSs are greater than those in normal metals by two or three orders of magnitude, which provides very intense electron scattering. At room temperatures, this disappears, because of phonons smearing the f-band. However, in the CHF particle, even at room temperatures, the intense electron scattering and narrow f-band could be kept.[18] For that, the CHF particle should have the energy gap E_g between the upper edge of the f-band and the nearest unoccupied electron state in the band of light electrons (Fig. 10), with the condition $[(\Gamma_f/2) + E_g] > \mathrm{kT} = 26\,\mathrm{meV}$. Such CHF nanoparticles could be effective THz-to-IR converters in a long-wavelength part of the THz range.

At room temperatures, the electron DOS within the f-band appears as in Fig. 10, where Γ_f is the width of the f-band, and $\Gamma_f \sim 10 - 100$ K (in energy units: $\Gamma_f \sim 8.7 \cdot 10^{-4} - 8.7 \cdot 10^{-3}$ eV). Photons can excite the f-electrons if their energies are multiple of (Γ_f/N), i.e., (Γ_f/N), $2 \cdot (\Gamma_f/N)$, $3 \cdot (\Gamma_f/N)$, ..., $(\Gamma_f/2)$, where N is the number of atoms in the CHF particle.

When reducing the number N, the energy distances between electron levels are increased: as $\Delta E_F/N$ in the band of light electrons, and as $\Delta E_f \sim \Gamma_f/N$ in the band of heavy electrons. Then, for the f-band to be conserved, i.e., for the sum of energies $[(\Gamma_f/2) + E_g]$ to be more than kT, the number N should meet the inequality: $N \leq E_F/\mathrm{kT}$. Assume that $E_F \approx 10$ eV. Then $N \leq 385$, and a particle's size would be about several nanometers.

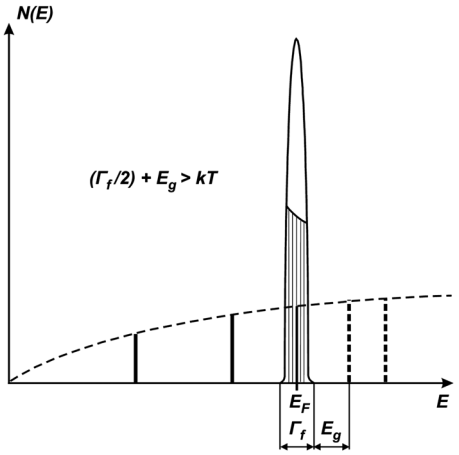

Fig. 10 Electron density of states versus electron energy in a CHF nanoparticle at room temperature (See Ref. 18). The vertical dotted lines above E_F show unoccupied states of light electrons.

With $\Gamma_f \sim 8.7 \times 10^{-4} - 8.7 \cdot 10^{-3}$ eV, the value of ΔE_f is within a range: $\Delta E_f \sim \Gamma_f / N \sim 2.3 \cdot 10^{-6} - 2.3 \cdot 10^{-5}$ eV. Thus, f-electrons could absorb photons with energies: $2.3 \cdot 10^{-6}$, $4.6 \cdot 10^{-6}$, $6.9 \cdot 10^{-6}$, ..., $4.3 \cdot 10^{-4}$ eV. These estimates are for the lower value of Γ_f. For the upper value of Γ_f, the photon energies able to be absorbed are as follows: $2.3 \cdot 10^{-5}$, $4.6 \cdot 10^{-5}$, $6.9 \cdot 10^{-5}$, ..., $4.3 \cdot 10^{-3}$ eV. These energies correspond to frequencies covering a range from 0.555 GHz to ~1 THz. Summarizing, we conclude that the long-wavelength THz photons could be effectively converted to heat by using the CHF nanoparticles in the THz-to-IR converter.

Acknowledgments

We are thankful to Dr. N. J. Kairyev for helpful discussions. Contributions of co-authors to this article are as follows: K.A.M.—a concept of the approach and estimations, V.M.L. and P.V.K.—calculations of data given in Figs. 5–7, A.K.K.—experimental measurements of transmittances (data given in Figs. 8 and 9).

References

1. Infrared Cameras Inc., "Mirage P-Series Infrared Thermal Imaging Camera," http://www.infraredcamerasinc.com/infrared-camera-Mirage.html (accessed 8 December 2012).
2. TYDEX® J.S.Co., "THz Lenses, THz Materials, and THz Low Pass Filters," in http://www.tydexoptics.com/en/products/thz_optics/ (accessed 8 December 2012).
3. A. Luukanen et al., "Measured performance of a high-resolution passive video-rate sub-millimeter-wave imaging system demonstrator for stand-off imaging," *Proc. SPIE* **8362**, 836209 (2012), http://dx.doi.org/10.1117/12.924166.
4. A. Luukanen et al., "Design and performance of a passive video-rate THz system demonstrator," *Proc. SPIE* **8022**, 802207 (2011), http://dx.doi.org/10.1117/12.883865.
5. E. Grossman et al., "Passive terahertz camera for standoff security screening," *Appl. Opt.* **49**(19), E106–E120 (2010), http://dx.doi.org/10.1364/AO.49.00E106.
6. S. A. Kuznetsov et al., "Bolometric THz-to-IR converter for terahertz imaging," *Appl. Phys. Lett.* **99**(2), 023501 (2011), http://dx.doi.org/10.1063/1.3607474.
7. S. A. Kuznetsov et al., "THz imaging system based on THz-to-IR converter," *Technisches Messen* **78**(11), 526–532 (2011), http://dx.doi.org/10.1524/teme.2011.0208.
8. S. A. Kuznetsov et al., "Matrix structure of metamaterial absorbers for multispectral terahertz imaging," *PIER* **122**, 93–103 (2012), http://dx.doi.org/10.2528/PIER11101401.

9. M. G. Kresch et al., "Neutron scattering measurements of phonons in nickel at elevated temperatures," *Phys. Rev. B* **75**(10), 104301 (2007), http://dx.doi.org/10.1103/PhysRevB.75.104301.
10. M. G. Kresch, "Temperature dependence of phonons in elemental cubic metals studied by inelastic scattering of neutrons and X-rays," PhD Thesis, California Institute of Technology, Pasadena, CA (2009).
11. P. Ziesche und and G. Lehmann, *Ergebnisse in der Elektronentheorie der Metalle*, Akademie-Verlag, Berlin (1983).
12. S. Hüfner, G. K. Wertheim, and J. H. Wernick, "X-Ray photoelectron spectra of the valence bands of some transition metals and alloys," *Phys. Rev. B* **8**(10), 4511–4524 (1973), http://dx.doi.org/10.1103/PhysRevB.8.4511.
13. C. V. Pandya et al., "Lattice mechanical properties of Pd, Pt and Ni—A Model potential approach," *J. Korean Phys. Soc.* **38**(4), 377–383 (2001), http://dx.doi.org/10.3938/jkps.38.377.
14. N. W. Ashcroft and N. D. Mermin, *Solid State Physics*, Saunders College Publishing, Harcourt College Publishers, Fort Worth (1976).
15. W. E. Schiesser, *The Numerical Method of Lines: Integration of Partial Differential Equations*, Academic Press, San Diego (1991).
16. V. M. Lelevkin et al., *Modelirovanie Mikrovolnovogo Nagreva Vody (The modeling of microwave heating of water)*, V. M. Lelevkin, Ed., KRSU, Bishkek (2009).
17. P. Keblinski et al., "Limits of localized heating by electromagnetically excited nanoparticles," *J. Appl. Phys.* **100**(5), 054305 (2006), http://dx.doi.org/10.1063/1.2335783.
18. K. A. Moldosanov, "Nanosplavy s tyazholymi fermionami kak detektory terahertsovogo izlucheniya ("Heavy-fermion nanoalloys as detectors of terahertz radiation")," *RENSIT: Radioelectronics. Nanosystems. Information Technol.* **3**(1), 102–105 (2011).
19. M. C. Kemp, "Explosives detection by terahertz spectroscopy—a bridge too far?," *IEEE Trans. Terahertz Sci. Tech.* **1**(1), 282–292 (2011), http://dx.doi.org/10.1109/TTHZ.2011.2159647.
20. G. R. Stewart, "Heavy-fermion systems," *Rev. Mod. Phys.* **56**(4), 755–787 (1984), http://dx.doi.org/10.1103/RevModPhys.56.755.

Kamil A. Moldosanov graduated from the physical faculty of the Lomonosov Moscow State University, USSR, in 1973. After having worked at different R&D institutions at physicist-engineer positions, notably at the Kurchatov Institute of Atomic Energy in Moscow (1973 to 1982), the Special Design Office of the Space Research Institute of the USSR Academy of Sciences in Frunze (1982 to 1991), OKB Aalam in Bishkek, Kyrgyz Republic (1991 to 2002), and APIT Corp. in Strasbourg, France (2003 to 2006), he became senior researcher at the Kyrgyz-Russian Slavic University, Bishkek, Kyrgyz Republic. His research interests cover low-reflectivity coatings, instruments for space plasma research, and applications of metal nanoparticles.

Valery M. Lelevkin graduated from the physical faculty of the Kyrgyz State University, Frunze (now Bishkek), Kyrgyzstan, in 1968 and got his PhD in physical and mathematical sciences in 1975. In 1990, he defended a doctor of sciences dissertation in heat and molecular physics. He is the author of more than 200 papers on theoretical physics, plasma physics, gas discharge physics, and electromagnetic radiation-substance interactions. He was a supervisor of studies in 15 PhD theses and 4 doctor of sciences dissertations. He is now the pro-rector of the Kyrgyz-Russian Slavic University, Bishkek, Kyrgyzstan.

Peter V. Kozlov graduated from the physical faculty of the Kyrgyz State University, Frunze (now Bishkek), Kyrgyzstan, in 1976 and defended his PhD thesis in 1985. He is the author of more than 60 articles in plasma physics. His research interests also cover computer modeling and numerical calculations of processes in thermal physics. After having worked at the Institute of Physics and Mathematics of the Kyrgyz Academy of Sciences and at the Computation Center of the Kyrgyz Republic, he became senior lecturer in computation mathematics and computer modeling at the Kyrgyz-Russian Slavic University, Bishkek, Kyrgyzstan.

Andrey K. Kaveev graduated from the physics and engineering faculty of the Saint Petersburg State Technical University, Russia, in 2001 and got his PhD in physical and mathematical sciences in 2005. He developed a number of experimental techniques for studying heterostructures on silicon. After having worked at the A. Ioffe Physics and Engineering Institute as a researcher, he became the R&D department manager at the TYDEX® J. S. Company in Saint Petersburg, Russia, where he is engaged in research in the field of terahertz optics. He is the author of more than 15 papers in peer-reviewed journals.